AFRL-RX-WP-TP-2009-4122

NbTiSiMo-X ALLOYS–COMPOSITION, MICROSTRUCTURE REFINEMENT AND PROPERTIES (PREPRINT)

Y-W. Kim, S. Menon, and C. Woodward

Metals Branch
Metals, Ceramics, and NDE Division

MARCH 2009

AIR FORCE RESEARCH LABORATORY
MATERIALS AND MANUFACTURING DIRECTORATE
WRIGHT-PATTERSON AIR FORCE BASE, OH 45433-7750
AIR FORCE MATERIEL COMMAND
UNITED STATES AIR FORCE

REPORT DOCUMENTATION PAGE

Form Approved
OMB No. 0704-0188

1. REPORT DATE *(DD-MM-YY)*	2. REPORT TYPE	3. DATES COVERED *(From - To)*
March 2009	Conference Paper Preprint	

4. TITLE AND SUBTITLE
NbTiSiMo-X ALLOYS–COMPOSITION, MICROSTRUCTURE REFINEMENT AND PROPERTIES (PREPRINT)

5a. CONTRACT NUMBER
In-house

5b. GRANT NUMBER

5c. PROGRAM ELEMENT NUMBER
62102F

6. AUTHOR(S)
Y-W. Kim and S. Menon (UES)
C. Woodward (AFRL/RXLMD)

5d. PROJECT NUMBER
4347

5e. TASK NUMBER
RG

5f. WORK UNIT NUMBER
M0241000

7. PERFORMING ORGANIZATION NAME(S) AND ADDRESS(ES)

UES
Materials & Processes
Dayton, OH 45432

Metals Branch (AFRL/RXLMD)
Metals, Ceramics, and NDE Division
Materials and Manufacturing Directorate
Wright-Patterson Air Force Base, OH 45433-7750
Air Force Materiel Command, United States Air Force

8. PERFORMING ORGANIZATION REPORT NUMBER
AFRL-RX-WP-TP-2009-4122

9. SPONSORING/MONITORING AGENCY NAME(S) AND ADDRESS(ES)
Air Force Research Laboratory
Materials and Manufacturing Directorate
Wright-Patterson Air Force Base, OH 45433-7750
Air Force Materiel Command
United States Air Force

10. SPONSORING/MONITORING AGENCY ACRONYM(S)
AFRL/RXLMD

11. SPONSORING/MONITORING AGENCY REPORT NUMBER(S)
AFRL-RX-WP-TP-2009-4122

12. DISTRIBUTION/AVAILABILITY STATEMENT
Approved for public release; distribution unlimited.

13. SUPPLEMENTARY NOTES
Conference paper proceedings preprint submitted to the TMS 2009 Annual Meeting. PAO Case Number: 88 ABW-2008-0810; Clearance Date: 04 Nov 2008. The U.S. Government is joint author of this work and has the right to use, modify, reproduce, release, perform, display, or disclose the work.

14. ABSTRACT
Advanced NbTiSi-X alloys have demonstrated very high RT strength levels (compressive yield strength approaching 1,800MPa) and excellent high-temperature strength retention (~1,200MPa at 1,000°C and over 500MPa at 1,200°C). Unfortunately, these alloys have an inhomogeneous size and spatial distribution of silicides, low fracture strength under tension (<300MPa) at all temperatures, and low oxidation resistance. The high volume fraction and non-uniform size distribution of silicides were considered to be responsible for the poor fracture resistance. In this work we attempt to refine the microstructure of cast alloys and to increase oxidation resistance by introducing Mo and adjusting other alloying additions. In focused efforts, we explored highly refined near-eutectic alloys, NbTiSiMo-Y, that showed excellent compression flow behavior. Further chemistry adjustments were made for balanced improvements, and cast alloys in homogenized material forms were evaluated for fracture to find that increases in fracture resistance without major chemistry modification are limited in the current alloy system.

15. SUBJECT TERMS
Nb-base Silicides, Chemistry Modification, Refinement, Fracture, Oxidation Resistance

16. SECURITY CLASSIFICATION OF:			17. LIMITATION OF ABSTRACT:	18. NUMBER OF PAGES	19a. NAME OF RESPONSIBLE PERSON (Monitor)
a. REPORT	b. ABSTRACT	c. THIS PAGE			Christopher F. Woodward
Unclassified	Unclassified	Unclassified	SAR	20	19b. TELEPHONE NUMBER *(Include Area Code)* N/A

Standard Form 298 (Rev. 8-98)
Prescribed by ANSI Std. Z39-18

NbTiSiMo-X ALLOYS – COMPOSITION, MICROSTRUCTURE REFINEMENT AND PROPERTIES

Y-W. Kim[1], S. Menon[1], C. Woodward[2]

[1]UES-Materials & Processes, Dayton, OH 45432
[2]AFRL/RXLMD, Wright-Patterson AFB, OH 45433

Keywords: Nb-base Silicides, Chemistry Modification, Refinement, Fracture, Oxidation Resistance

Abstract

Advanced NbTiSi-X alloys have demonstrated very high RT strength levels (compressive yield strength approaching 1,800MPa) and excellent high-temperature strength retention (~1,200MPa at 1,000°C and over 500MPa at 1,200°C). Unfortunately, these alloys have an inhomogeneous size and spatial distribution of silicides, low fracture strength under tension (<300MPa) at all temperatures, and low oxidation resistance. The high volume fraction and non-uniform size distribution of silicides were considered to be responsible for the poor fracture resistance. In this work we attempt to refine the microstructure of cast alloys and to increase oxidation resistance by introducing Mo and adjusting other alloying additions. In focused efforts, we explored highly refined near-eutectic alloys, NbTiSiMo-Y, that showed excellent compression flow behavior. Further chemistry adjustments were made for balanced improvements, and cast alloys in homogenized material forms were evaluated for fracture to find that increases in fracture resistance without major chemistry modification are limited in the current alloy system.

Introduction

Nb based silicide, Nb_5Si_3, has attractive structural properties that include high melting temperature (2520°C), low density, high stiffness, good high-temperature strength retention and remarkable creep and oxidation resistance [1, 2]. However, due to its intrinsic brittleness this silicide will require toughening by a second phase, for example a Nb solid-solution (Nb-ss), in order for this alloy to be considered for rotational component applications [3-5]. The binary Nb–Si alloy system exhibits a wide two-phase region of Nb_5Si_3 and Nb-ss with eutectic and eutectoid reactions offering a variety of microstructures to control [5, 6]. The binary or simple ternary Nb-Ti-Si alloys, generating Nb-ss /Nb_5Si_3 in-situ composites, showed reasonable RT fracture resistance and processibility, but inadequate or poor high temperature strength, creep and oxidation resistance. Extensive research activities during the period of 1990's and early 2000 in understanding the mechanical properties (strength and fracture) of Nbss /Nb_5Si_3 in-situ composites, resulted in the development of multi-component Nb-Ti-Si-X(Cr, Al, Hf, Sn, Ge) alloys having improved strength levels and high-temperature mechanical properties [7-12]. Unfortunately, these improvements were achieved at the expense of processibility and fracture resistance [1, 13, 14], and their oxidation resistance remains inadequate or poor [15, 16]. The fracture resistance of the Nb/Nb_5Si_3 composites is principally controlled by the deformation and fracture behavior of the Nb-ss phase, while the high-temperature strength and creep resistance are governed by the Nb_5Si_3 phase [17]. The Nb-Mo-Si system contains a new eutectic (Nb+ Nb_3Si) valley, L→ Nbss + Silicides, over a wide range of Mo content (3-45at%) [18]. Mo not

only promotes eutectic reactions leading to very fine eutectic structures but also effectively solid solution hardens the beta phase (Nb-ss) at RT and less effectively at high temperatures. At near-eutectic compositions the fracture toughness of the alloys in this system is shown to have improved fracture resistance over the Nb-Ti-Si-X alloys [10]. Our preliminary experiments indicated that Mo additions might slow down oxidation of the composites.

Fracture resistance of Nb-ss/Nb_5Si_3 composites is known to be sensitive to the volume fraction and composition of constituent phases as well as microstructure [2, 5], the latter of which is considered to be the controlling factor for a given alloy system. High temperature strength (including creep resistance) is expected to depend on the same factors but the opposite ways, that is: higher the volume fraction of silicides and stronger the beta phase, greater the creep resistance.

The present experiment is aimed to explore Nb-Ti-Si-Mo-Zr alloys, through modification of current Nb-Ti-Si alloys by replacing some of Nb or Ti with Mo and Zr, such that their compositions become near eutectic and that they are decomposed to fine, uniform globular Nb+ Nb_5Si_3 composites upon high temperature annealing treatments having enhanced strength and fracture behavior as well as improved oxidation resistance.

Experiment

Four groups of alloys were investigated for microstructure refinement, oxidation resistance, strength variation with temperature, and fracture behavior as a function of temperature. Their compositions (in at%) are listed in Table 1. All alloys are Mo modified, except for alloys M0 and A2, and were produced in arc-melted cigar forms weighing 300g. Coupon samples from Group I alloy cigars were given a homogenization treatment at 1500°C/24h and either evaluated for microstructure evolution and/or oxidation resistance at 1000°C under cyclic exposure conditions. Alloys M0, M1 and M2 contain a high Ti content (24at%) and a low Si content (13at%), but a differing amount of Mo addition (0, 14 and 19at%, respectively). This results in widely varying Nb contents. On the other hand, alloy M3 is featured a drastically reduced Ti content and significantly increased Al amount. Group II alloys, featured by significantly differing Ti as well as Mo contents and absence of Cr, were evaluated for microstructure and phase distribution in as cast condition as well as after a homogenization treatment at 1,500°C for 100h. Group III alloys, formulated based on the evaluation results of group I and II alloys to have a constant (Zr+Mo) content, were characterized for their microstructures and used for compression testing at room temperature (RT), 1000°C and 1200°C. Group IV alloys were formulated to have relatively small Ti contents, negligible Al amounts and varying Zr additions, which end up a wide range of Nb contents. The alloy cigars were HIP'ed at 1500°C/6h/173MPa and given a homogenization treatment at 1500°C/24h in an argon furnace. Compression testing was conducted on 3mm diameter cylindrical samples at RT, 800°C, 1,000°C, 1100°C and 1200°C. 4-point bend testing was conducted on smooth bend bars at RT, 800°C, 1,000°C, 1,100°C and 1,200°C. 3-point bend bar testing was carried out on single edge notched bar (SENB) at RT. Duplicate tests were conducted for each test condition. In order to put the current alloys in context with previous work a state-of-the-art alloy from early 2000, AF02 (44.7Nb-24Ti-19Si-5.0Cr-2.0Al-3.5Hf-0.8Sn-1.0W), was also produced in an arc melted cigar form and tested using similar procedures. Whenever needed, microstructure evaluation was carried out, and micro-composition analysis was conducted on fine eutectic areas of homogenized samples of selected alloys using the EPMA technique. The average composition of the eutectic area was compared with the corresponding alloy composition. Coupon samples for Alloy E69 and group IV alloys were cyclically exposed

in air between RT and elevated temperatures including 800°C, 1,000°C, 1,100°C and 1,200°C. The accumulated expose times were up to 230h, and weight changes were measured at RT every after exposure.

.

Table 1: Three groups of alloys and their compositions (at%) selected for the present study

Group	Alloy	Nb	Ti	Si	Cr	Al	Hf	Sn/Ge	Zr	Mo
I	M0	48.5	24	13	9.5	2	2	1/0	-	-
	M1	32	24	13	9	5	2	1/0	-	14
	M2	29	25	13	9	2	2	1/0	-	19
	M3	44	12	14	5	10	5	-	-	10
II	E1	45.5	12.5	19.0	-	3.0	3.0	-	3.0	15.0
	E2	47.5	20.0	16.0	-	3.0	3.0	-	3.0	7.5
III	2D	43.5	17.5	12.5	5.0	3.0	3.0	1.5/3.5	3.0	7.5
	E71	42.0	17.5	16.0	5.0	3.0	3.0	0/3	3.0	7.5
	E69	50.0	12.5	16.0	5.0	3.0	3.0		3.0	7.5
IV	DE	51.3	11.6	18.5	3.8	0.5	2.1	-	3.8	8.4
	LE	55.4	9.0	19.2	2.3	0.1	1.8	-	3.1	9.1
	DE1	46.0	12.5	18.5	5.0	1.0	2.0	-	5.0	10.0
	LE1	40.0	12.5	18.5	5.0	1.0	3.0	-	10.0	10.0

Results and Discussion

Group I Alloys

In Group I alloys, alloy M0 exhibits uneven but relatively fine microstructures in a homogenized condition (1500°C/24h) under back-scattered electron imaging (BEI), Figure 1a. There are a mixture of beta phase (imaged bright) and silicides particles (imaged gray) with small amounts of scattered Cr_2Nb type Laves phase (imaged dark) patches. Judged from the morphology and scale, the M0 alloy composition was solidified by dendritic growth. With Mo additions at the expense of Nb content, eutectic solidification takes place, as shown in Figure 1b for a homogenized alloy M1 sample. Significant refinement and uniformity in microstructure with the absence of primary silicides in the M1 alloy cigar indicates that the eutectic solidification with a low Si content (13%, Table 1) is free of primary silicides. Drastic microstructure refinement observed in alloy M2 suggests that Mo additions effectively refine the eutectic microstructure (both beta phase grains and silicides) in this composition range. It appears that the Mo addition also reduces the volume fraction of Laves phase. Figure 2 shows weight changes of group I alloys during cyclic oxidation at 1000°C and room temperature (RT). Reducing the Nb content in alloy M0 with an addition of 19%Mo (alloy M2) removed (or significantly reduced) the tendency of oxide spallation. Nevertheless, oxidation continued to take place at increasing rates on alloy M2. Alloy M3 with the addition of 10at% Mo and 10at% Al at the expense of Ti and Nb appears remarkably resistant to oxidation. The increase in Al content is expected to yield a substantial amount of oxidation resistant Nb_3Al at the expense of beta phase and should produce alloys with much better oxidation resistance than the other alloys

in Table 1. This expected phase redistribution is considered to end up with the enhanced oxidation resistance.

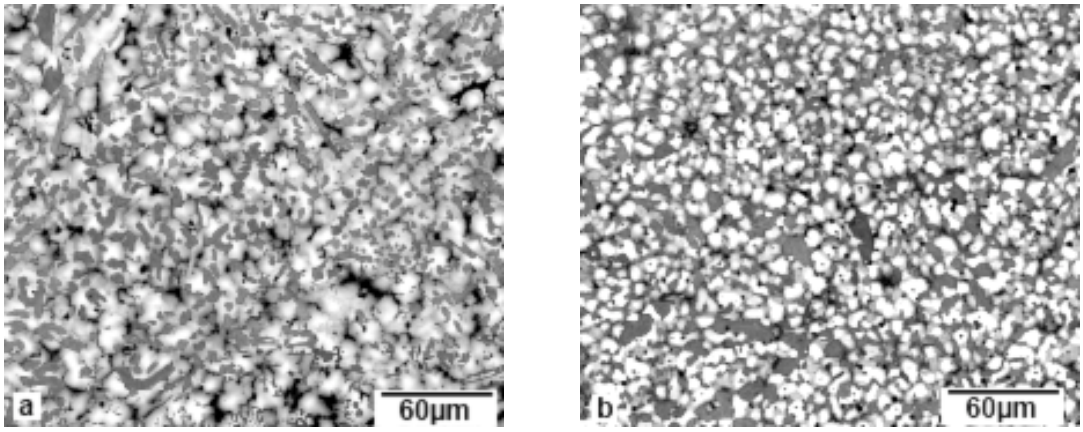

Figure 1: BEI microstructures of arc-melted Group I alloys, M0 (no Mo) and M1 (containing 14% Mo) after annealing at 1500°C for 24h, showing the effect of Mo on the refinement of dendrite microstructure in M0 (a) and eutectic microstructure in alloy M1 (b).

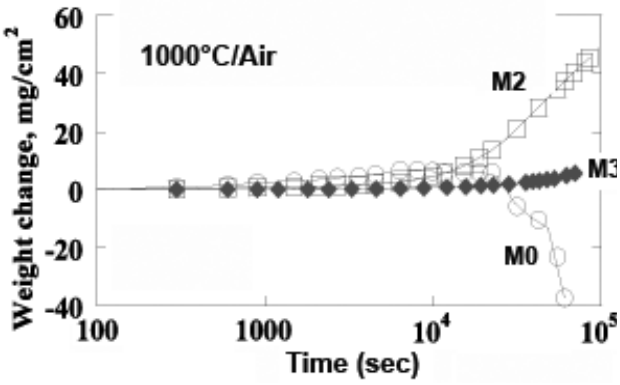

Figure 2: Weight changes of group I alloys, Mo, M2 and M3, under cyclic exposure at 1000°C-RT, showing the effect of (Mo + Al) addition effect on oxidation resistance

Group II Alloys

Group II alloys showed eutectic microstructures typical of the Nb-ss/Nb_5Si_3 system containing Mo, and Figure 3 shows that of alloy E2 as an example in the as cast condition and after a heat treatment at 1500°C for 100h. The heat treatment decomposed the as-cast fine eutectic structure (Figure 3a) to a mixture of continuous beta matrix (imaged bright) and silicide particles (imaged dark) that are coarser but fairly uniformly distributed (Figure 3b).

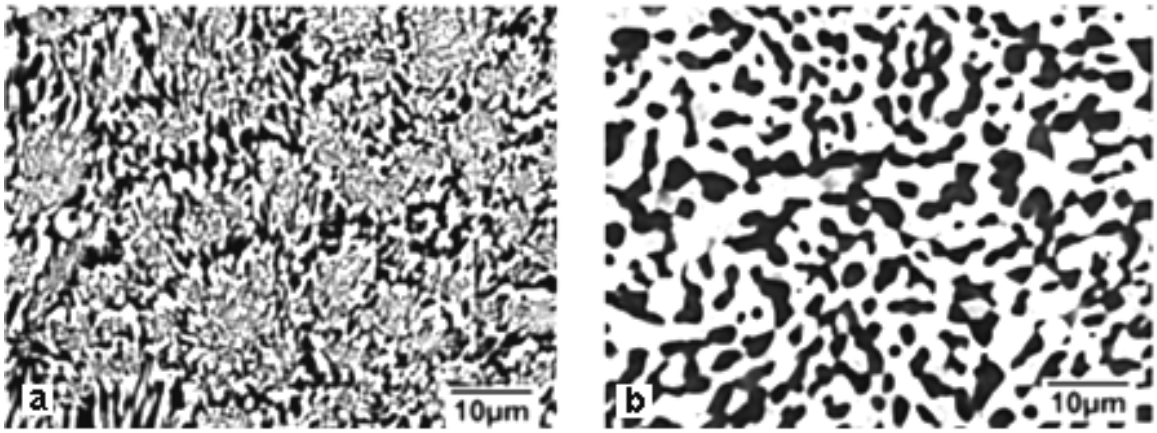

Figure 3: Typical BEI eutectic microstructures observed in Group II alloy, E2, in as-cast condition (a) and after heat treatment at 1500°C for 100h (b).

Group III Alloys

Among Group III alloys, eutectic E69 showed the best cyclic oxidation resistance at all temperatures after an annealing treatment (Figure 4a). Its weight changes occurring upon cyclic exposures at three different temperatures, plotted in Figure 4b, exhibit typical oxidation behavior: rapid oxidation and weight loss at low temperatures (<1000°C), remarkably slow oxidation rate at 1000°C, and accelerated oxidation (but still slower than that at 800°C) and spallation at 1200°C. The unusually rapid oxidation rate taking place at 800°C was explained by the cracking of silicides near the sample surface caused by the oxidation-induced internal stress in the beta phase [SM]. In this explanation, the compressive stresses built in the beta phase are relieved in the form of cracking of adjacent silicides which are still brittle at 800°C, leading to spallation of the oxide scale. At higher temperatures, it is assumed that the stress is built up to lesser degrees and also the silicides are capable of absorbing some of the strains. At 1200°C, the general oxidation appears to dominate the other effects. Alloy E69 responded to compression better than other group III alloys at all temperatures, as exemplified in Figure 5 for two temperatures, RT (a) and 800°C (b).

(a)

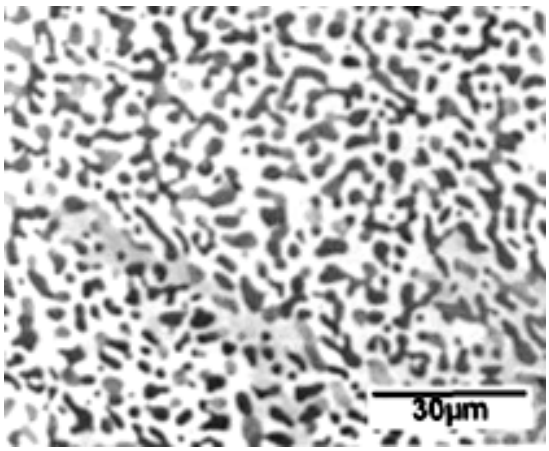

(b)

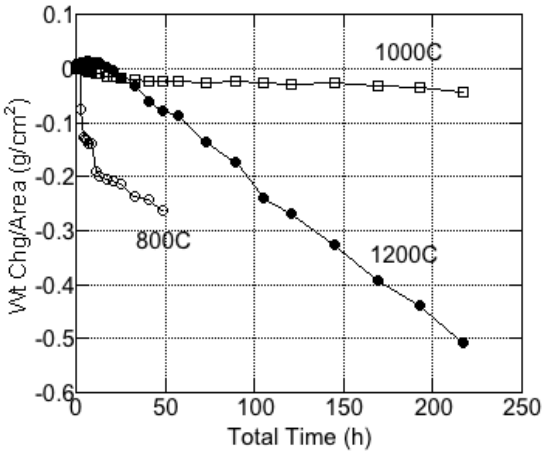

Figure 4: A near-eutectic Group 3 alloy, E69, showing the BEI microstructure of the eutectic area decomposed upon homogenization treatment at 1500°C for 24h (a) and weight changes under cyclic exposures at three different temperatures (b).

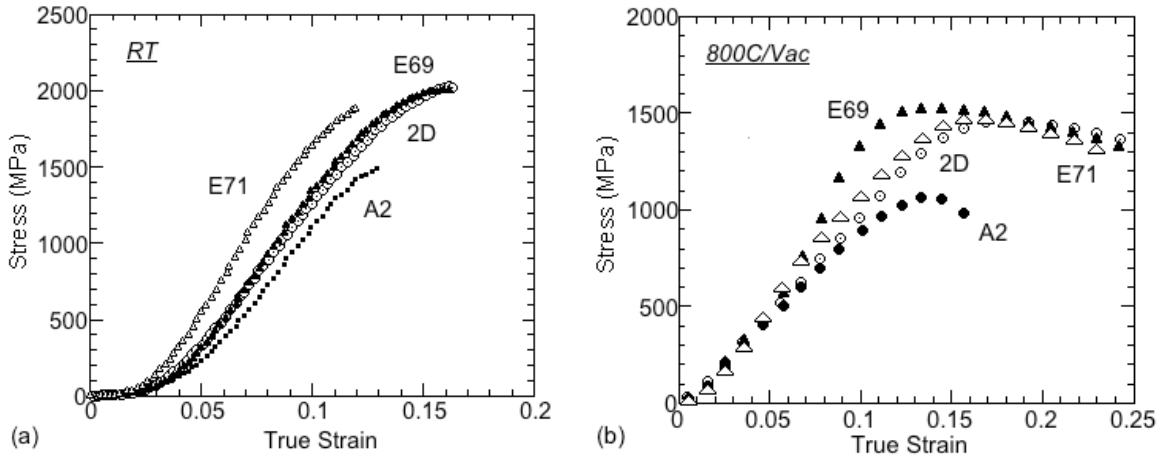

Figure 5: Compression flow curves of Group III Alloys, 2D, E69, E71 and A2, at RT (a) and 800°C (b)

Group IV Alloys

Based on the results from Group III, alloy E69 was selected as the baseline composition for formulating Group IV alloys. Coupon samples were prepared from the arc-melted cigars of E69 and Group IV alloys and given an annealing treatment at 1500°C for 24h. Figure 6 shows the BEI microstructures of the annealed Group IV alloys that consist of decomposed eutectic and primary silicides plates (imaged dark) along with coarse beta grains (imaged bright) for alloys DE (a), LE (b) and LE1 (d). The annealed alloy DE1 shows mainly decomposed eutectic structures, Figure 6c. Micro-composition analyses were conducted using the electron probe microanalysis (EPMA) technique by scanning a typical fine-microstructure area of 200µm x 100µm of teach of alloys samples (E69, DE1 and LE1) with a 10µm diameter electron beam. Each of the averaged compositions is supposed to represent the eutectic composition, and the results are listed in Table 2 along with the corresponding alloy compositions. Despite the presence of primary silicides even after the annealing treatment (Figure 6), the compositions of the eutectic areas are near respective alloy compositions. This might indicate that the eutectic reactions along the eutectic valleys are complex and difficult to achieve near-equilibrium solidification pathways.

Table 2: The Alloy Compositions and Eutectic Compositions (E) of E69, DE1 and LE1 Measured by EPMA

Alloy-E	Nb	Ti	Si	Cr	Al	Hf	Zr	Mo
E69	50.0	12.5	16.0	5.0	3.0	3.0	3.0	7.5
E69-E	49.2	12.8	16.6	4.4	2.9	3.3	3.0	7.8
DE1	46.0	12.5	18.5	5.0	1.0	2.0	5.0	10.0
DE1-E	44.6	13.3	18.4	4.6	1.1	2.0	5.2	10.8
LE1	40.0	12.5	18.5	5.0	1.0	3.0	10.0	10.0
LE1-E	40.4	12.5	17.6	5.0	1.1	3.0	9.3	11.1

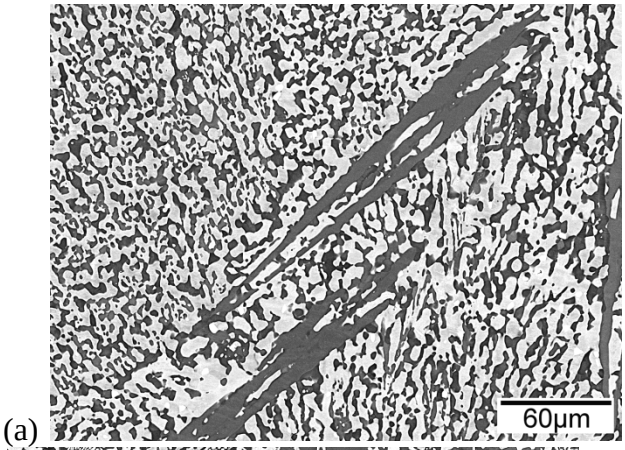

(a) (b)

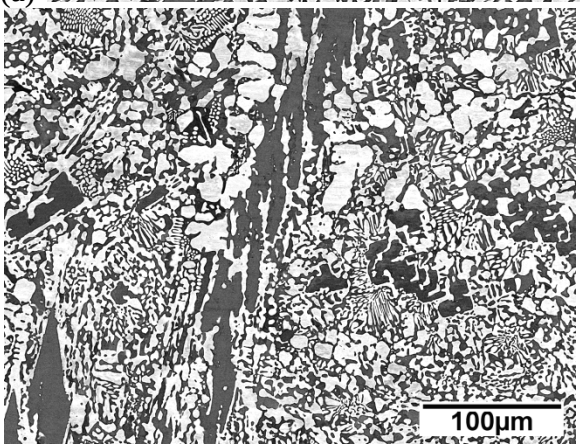

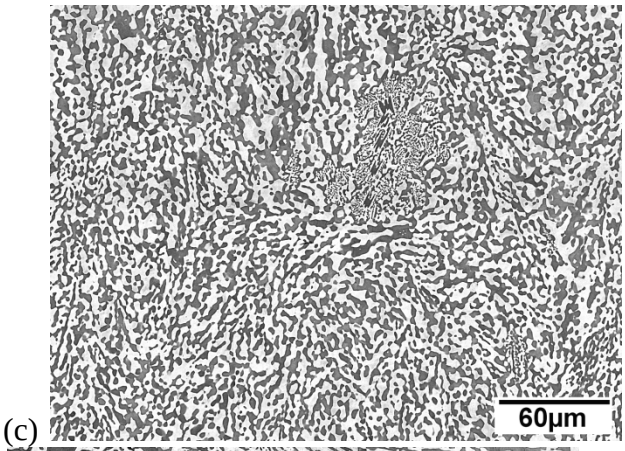

(c) (d)

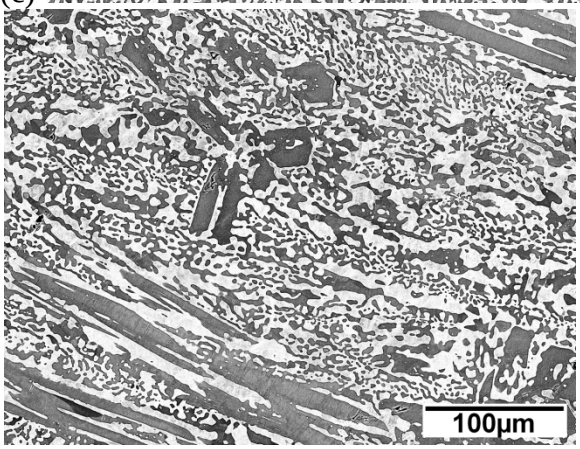

Figure 6: BEI microstructures of group 4 alloys, DE (a), LE (b), DE1 (c) and LE1 (d), after an annealing treatment (1500°C/24h) (c and d in next page)

Figure 7 illustrates the measured strengths (CS, CYS, SBFS and NBFS) of annealed Group 4 alloys and alloy AF02 (Nb-24Ti-19Si-5Cr-2Al-3.5Hf-0.75Sn-1W) at RT. The compression strength (CS) is defined as the ultimate strength under compression, CYS is the yield strength under compression, SBFS indicates smooth bar fracture stress under 4-pt bend testing, and NBFS is notched bend bar fracture stress under 3-pt bend testing. It is clear that the intrinsic strengths (CS and CYS) of the Group IV alloys at RT, as are those of E69, are significant, with CYS ranging from 1610 to 1830MPa, but that their tensile fracture strengths are measured to be less than 320MPa or 18% of the yield strengths. Furthermore, the notched tensile fracture strengths are less than 90MPa or only 5% or so of the yield strengths, demonstrating the alloys' manifest high notch sensitivity.

The variations of compressive strengths and smooth bar tensile fracture strengths of these alloys are shown as a function of temperature in Figure 8. All Group IV alloys show excellent high temperature strength retention up to 1200°C, as compared with those of AF02 and E69 alloys, Figure 8a. For example, alloy DE1 exhibited a CS (peak stress) of 630MPa and YS of 480MPa at 1200°C. Smooth bar tensile fracture strengths of Group IV alloys tend to increase gradually with temperature to reach as high as 500MPa at 1200°C, Figure 8b. The fluctuation of the fracture stresses is suggestive that variations in microstructure (e.g., large silicide plates in Figure 6) from sample-to-sample may play a role. To our knowledge this is the first report of gradual

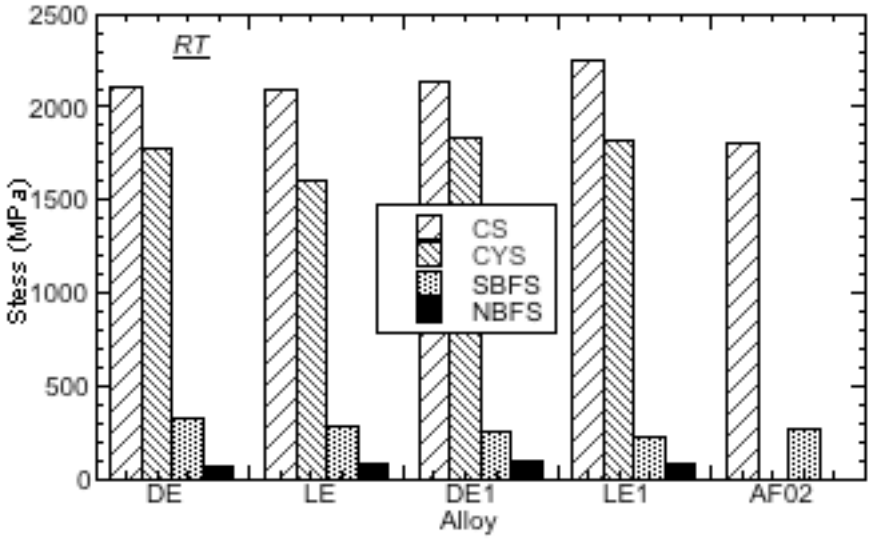

Figure 7: Various strengths of group IV alloys against those of alloy AF02 are shown, including compressive strength (CS) (either fracture strength or peak strength), compressive yield strength (CYS), 4-pt smooth bend bar fracture strength (SBFS), and 3-pt single notched bend bar fracture strength (NBFS). Drastically lowered fracture strengths under tension are apparent.

but significant increases in fracture resistance in this class of alloys. Typically the fracture stress remains constant before gradually dropping off at high temperatures, as shown for alloy AF02 in Figure 8c.

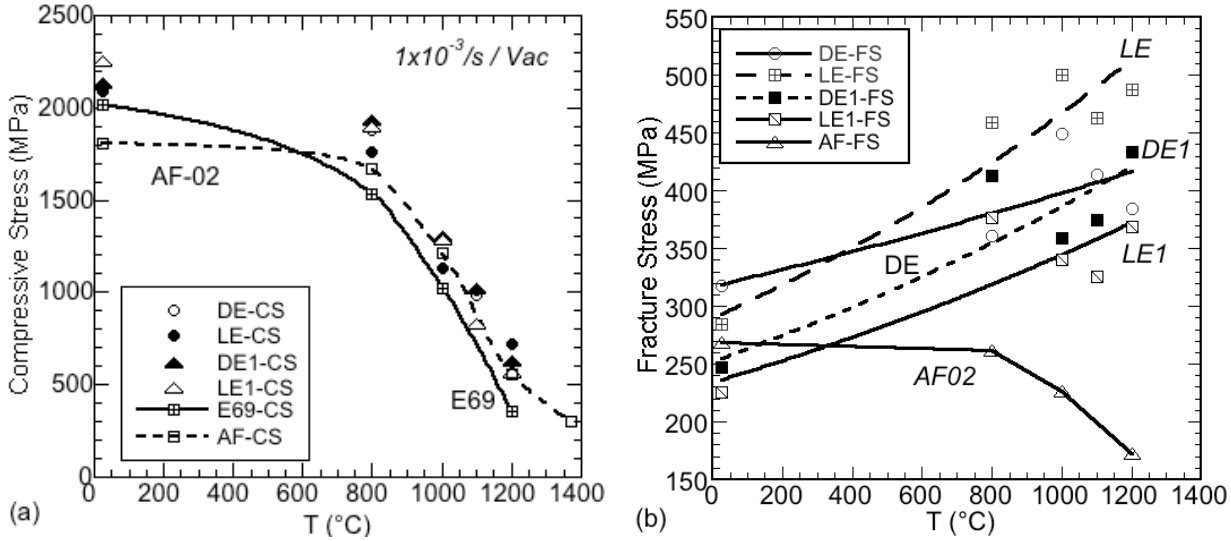

Figure 8: Compressive strengths of Group IV alloys as a function of temperature are plotted against those of alloys E69 and AF02 (a) and variations of the fracture strengths of Group IV alloys under tension with temperature are compared with those of E69 and AF02 (b).

Even at 1200°C, however, the fracture strengths do not appear to exceed the yield strength, as illustrated in Figure 9 for alloys DE1 and AF-02. Though not shown here, the AF02 composition is away from the eutectic and thus contains greater amounts of primary silicides, which likely produces lower fracture strengths than in DE1. Clearly, however, even DE1 having improved properties does not exhibit any plasticity under tension at temperatures up to 1200°C, meaning that the brittle-ductile-transition temperatures (BDTT) are higher than 1200°C for group IV alloys. It is expected that raising the fracture strengths to acceptable levels may be accomplished through controlling the microstructure, producing more uniform microstructure and controlling the size and spatial distribution of silicides such that the ductile beta phase areas are less constrained. Efforts in this area can be worthwhile, but the results from such a strategy may still be somewhat limited.

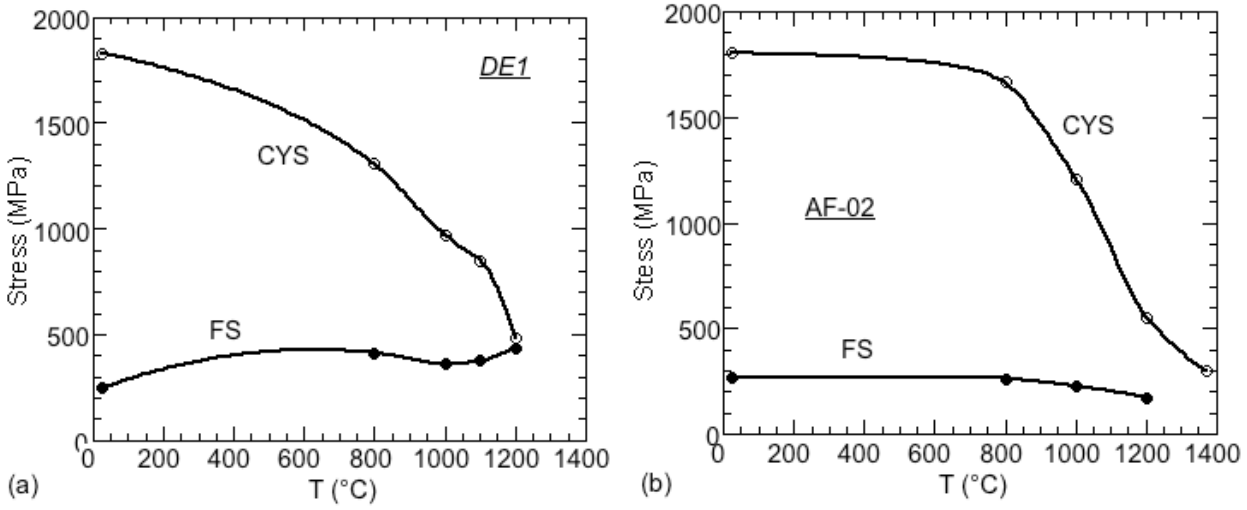

Figure 9: The variations of fracture strength measured under tension (FS) as a function of temperature are compared with those of yield strength measured under compression (CFY) for alloy DE1 (a) and AF02 (b)

Oxidation Resistance

Cyclic oxidation resistance of Group IV alloys, as measured by weight changes, is compared as a function of exposure time at different temperatures in Figure 10. Overall, the lowest oxidation resistance is seen at 800°C (Figure 10a), which has been explained earlier in terms of accelerated spallation of oxide scale due to cracking along oxygen-rich β/Nb_5Si_3 interfaces near the surfaces [15] as a means of relieving oxidation-induced residual stress buildup in the beta phase. Nevertheless, relatively significant enhancements of the oxidation resistance are apparent in alloys DE1 and LE over the baseline alloy E69. The major differences are that DE1 and LE contain greater (if not significant) amounts of Si and Mo, which will increase the volume fractions of silicides and increase Mo in the beta phase solution. On the other hand, the oxidation resistance in alloy LE1was not improved in spite of the same increase in Si and Mo, and that may then be related to an increased amount Zr addition (from 5% to 10% in Table 1). One possible explanation is that the additional Zr addition may further promote either internal stresses and/or spallation process.

At 1000°C, the highest oxidation resistance is seen (Figure 10b) for all alloys except for LE1. The oxidation resistance of DE1 is remarkable with a weight loss of only 7mg/cm^2 after 100h exposure in air. Minimal spallation takes place thanks to the absence of interfacial cracking, and slow oxygen penetration is assumed perhaps due to certain type of self-protective coating. At 1200°C, however, all alloys other than LE1 show accelerated weight losses with time at the same rate, Figure 10c. The maximum oxidation resistance on alloy LE1 happens at 1200°C, which is unexpected, and the significance is that LE1 having an additional 5at% Zr reduces the Nb content to 40at%, Table 1. It can be speculated that large amounts of dissolved Zr slow down oxygen diffusivity in the beta phase as well as oxygen penetration along the interfaces.

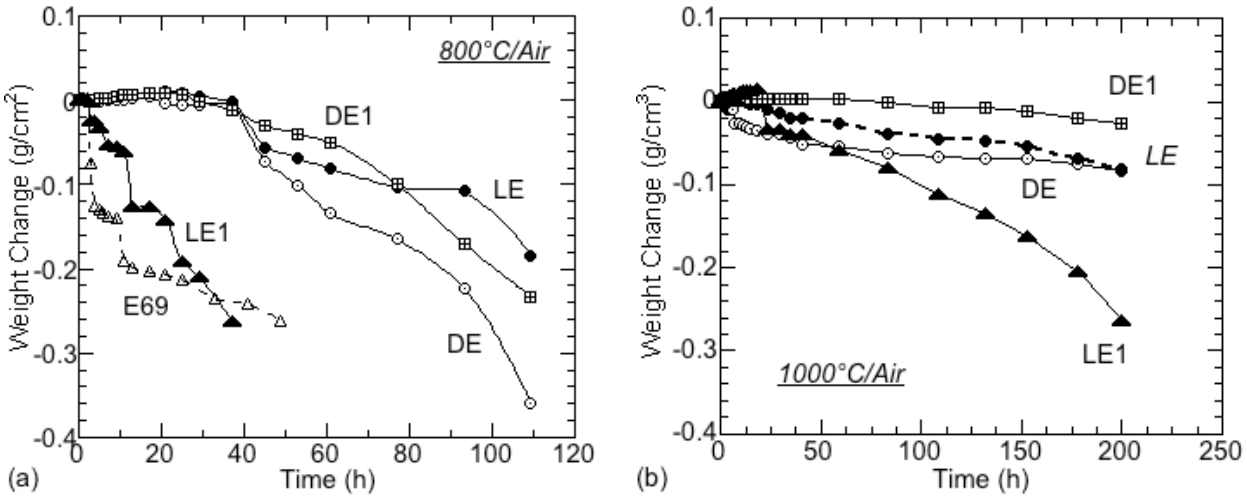

Figure 10 (Captions and an additional figure are in next page)

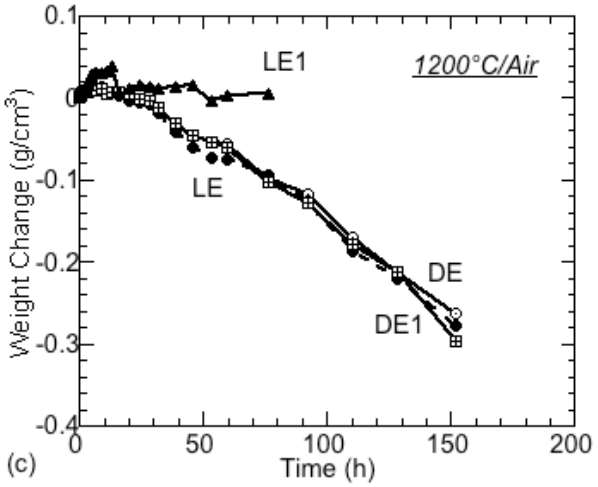

Figure 10: Weight changes on coupon samples of Group IV alloys as a function of cyclic exposure time at 800°C (a), 1000°C (b) and 1200°C (c)

The effect of increasing Zr content on the cyclic oxidation behavior is further illustrated in Figure 11, where the cyclic weight changes on alloy DE1 (a) and LE1 (b) are plotted as a function of exposure time at four different temperatures. LE1 is essentially the same as DE1, except for containing a greater amount of Zr (10at%), as compared to that (5at%Zr) in DE1. Alloy DE1 shows decreasing weight loss with increasing temperature to a minimum around 1000°C. In alloy LE1, the weight losses decrease as temperature increase up to 1200°C. Collectively, a few important aspects can be drawn from these observations. It is reasonably assumed that the oxidation resistance depends on the volume ratio between the beta phase and silicides, with the greater ratio the less oxidation resistant. For a given ratio, the rate is controlled by the cracking along the β/silicide interfaces, which is controlled by the internal residual stress produced by the beta phase during exposure and promoted by oxygen penetration along the interfaces. However, internal stress buildup becomes eased as temperature increases, and the ability to accommodate the internal strain of the beta phase is enhanced. Therefore, interfacial separation induced spallation is diminished at a certain temperature near 1000°C for alloys containing 5at% or less Zr. In this temperature range, the overall oxidation resistance remains high due to the presence of finely dispersed, high-volume silicide particles.

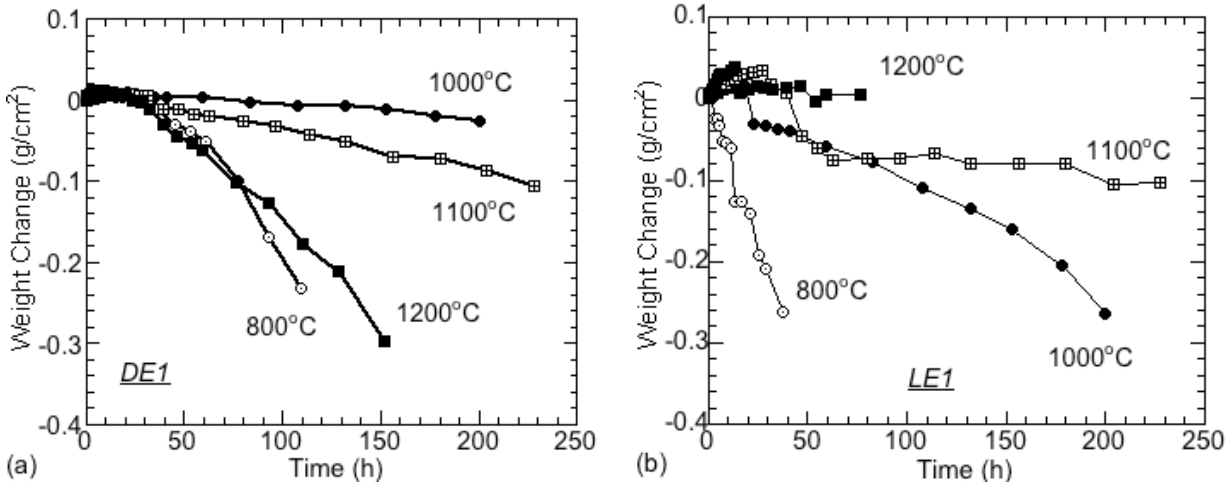

Figure 11: Effect of different Zr additions on the weight changes of coupon samples for alloys DE1 (with 5%Zr) (a) and LE1 (with 10%Zr) (b) as a function of exposure time at four different temperatures.

Increases in Zr content are likely to enhance the internal stress of beta phase, while the additions may slow oxygen ingress even at 1200°C (Figure 11b). The influence of the Zr additions on damaging oxide scale (cracking and spallation) on the 10at% Zr-containing LE1 must be far greater than on enhancing oxidation resistance at low temperatures such as 800°C. On the other hand, the increased oxidation resistance becomes more important as the cracking induced spallation is reduced with increasing temperature and eventually diminishing near 1000°C. This is clearly illustrated in Figure 11.

Summary and Conclusions

The present experimental study was aimed to develop Nb(β)/Nb_5Si_3 composite alloys that will have improved balance in mechanical properties and oxidation resistance. The strategy was to modify the chemistry of existing Nb-Ti-Si-X based alloys into a fine grained eutectic alloy system, Nb-Ti-Si-Y-Mo-Zr, where X and Y denote other alloying elements such as Al, Cr, Hf, Sn, etc. A series of alloy groups were produced in arc-melted cigar forms and given annealing treatments at 1500°C. Through evaluation of microstructure evolution and strength and oxidation behavior, alloy compositions were progressively refined to meet the microstructural objectives. Alloys in the final group were evaluated in detail for strengths under compression, fracture behavior under tension and cyclic oxidation resistance in the temperature range between RT and 1200°C. The evaluation results are summarized below.

1. Mo additions result in the refined microstructures in both as cast as well as annealed dendrite alloys and eutectic alloys. However, in Nb-Ti-Si-Mo alloys having 16at% or greater Si, suppressing the formation of coarse primary silicide plates is not practical even in eutectic alloys.

2. Remarkable intrinsic strength levels (yield strength YS ranging from 1600-1850MPa) were achieved with Mo additions, indicating that Mo solid solution strengthens the beta phase; however, adequate high temperature (>1000°C) strength retention required sufficient Si content (>17%), preferably around 19%. Lowering the Ti content (from 18 to 12%, for example) appears to enhance high temperature elongation.

3. Premature brittle fracture takes place under tension (measured by bend test) at all temperatures, with fracture strength (FS) being less than 0.2YS at RT and close to YS at 1200°C. The gradual increase in fracture resistance with temperature has not been reported in any other systems. Nevertheless, the overall fracture strengths are too low for any rotational applications. Pronounced notch sensitivity at RT was observed with the fracture strength on notched bend bars ranging from 70 to 90MPa.

4. Microstructure control to remove primary silicides is expected to enhance the fracture resistance. Judging from the present results, however, the improvements may still be inadequate for structural applications

5. All Nb-(9-12.5)Ti-(16-19)Si-Y-(7.5-10)Mo-(3-10)Zr alloys show the highest oxidation rates at low temperatures around 800°C. In these fine-grained alloys, this can be explained by the cracking or separation of β/Nb_5Si_3 interfaces due to the oxidation-induced residual stresses

produced in the beta phase, which then produces oxide spallation. The overall oxidation resistance therefore increases with temperature with the maximum occurring at 1000°C with 10Mo+5Zr additions and around 1200°C with 10Mo+10Zr additions.

6. Based on the properties and oxidation behavior, alloy DE1 (Ti-46Al-12.5Ti-18.5Si-5Cr-1 duAl-2Hf-5Zr-10Mo) is recommended as the baseline alloy for future development effort (in terms of balance in strength-temperature relations and oxidation resistance)

Acknowledgment

This research was supported under the Air Force Contract No. FA8650-04-D-5233.

References

[1] M.R. Jackson, B.P. Bewlay, R.G. Rowe, D.W. Skelly, H.A. Lipsitt, JOM 48 (1) (1996) 39.
[2] P.R. Subramanian, T.A. Parthasarathy, M.G. Mendiratta, D.M. Dimiduk, Scripta Metall. Mater. 32 (1995) 1227–1232.
[3] M.G. Mendiratta, D.M. Dimiduk, MRS Proc. on High-temperature Ordered Intermetallic Alloys III (MRS, Pittsburgh, PA.), 133 (1989) 441.
[4] D.L. Anton, D.M. Shah, MRS Proc. on Intermetallic Matrix Composites, (MRS, Pittsburgh, PA), 194 (1990) 45.
[5] M.G. Mendiratta, J.J. Lewandowski, D.M. Dimiduk, Metall. Trans. 22A (1991) 1573–1583.
[6] T.B. Massalski, et al., Binary Alloy Phase Diagrams, ASM, Metals Park, Ohio, 1992.
[7] J. Sha, H. Hirai, T. Tabaru, A. Kitahara, H. Ueno, S. Hanada, Metall. Mater. Trans. 34A (2003) 85–94.
[8] W.Y. Kim, H. Tanaka, S. Hanada, Intermetallics 10 (2002) 625–634.
[9] J. Sha, H. Hirai, T. Tabaru, A. Kitahara, H. Ueno, S. Hanada, Mater. Sci. Eng. A343 (2003) 282–289.
[10] W.Y. Kim, H. Tanaka, A. Kasama, S. Hanada, Intermetallics 9 (2001) 827–834.
[11] M.G. Mendiratta, D.M. Dimiduk, Metall. Trans. 24A (1993) 501–504.
[12] J. Sha, H. Hirai, T. Tabaru, A. Kitahara, H. Ueno, S. Hanada, Metall. Mater. Trans. A 34 (2003) 2861–2871.
[13=1] Jackson MR, Bewlay BP, Rowe RG, Skelly DW, Lipsitt HA. JOM 1996; 1:39.
[13] Giabara R, Chang H, Czarnik C, Edwards K, Misra A., in Structural Intermetallics, eds. Darolia R, et al., TMS, Warrendale, PA: TMS, 1993. p. 561.
[14] Kajuch J, Short J, Lewandowsky JJ. Acta Metall 1995; 43:1955.
[15] E. S. K. Menon, M. G. Mendiratta and D. M. Dimiduk, in Structural Intermetallics 2001, eds. K. J. Hemker, D. M. Dimiduk, et al. (TMS, 2001) 591-600.
[16] S. Menon, in Nb for High Temperature Applications, eds. Y-W. Kim and T. Carneiro, TMS (2004),
[17] P.R. Subramanian, M.G. Mendiratta, D.M. Dimiduk, JOM 48 (1) (1996) 33.
[18] C.L. Ma, Y. Tan, H. Tanaka, A. Kasama, R. Tanaka, Y. Mishima, S. Hanada, Y. Mishima, S. Hanada, Mater. Trans. JIM 41 (2000) 1329.